Large tunable FMR frequency shift by magnetoelectric coupling in oblique-sputtered $Fe_{52.5}Co_{22.5}B_{25.0}$/PZN-PT multiferroic heterostructure*

Zhi-Peng Shi(时志鹏), Xiao-Min Liu(刘晓敏), and Shan-Dong Li(李山东)†

College of Physics, Key Laboratory of Photonics Materials and Technology in Universities of Shandong, and Laboratory of Fiber Materials and Modern Textile, the Growing Base for State Key Laboratory, and National Demonstration Center for Experimental Applied Physics Education, Qingdao University, Qingdao 266071, *China*

(Received 11 April 2017; revised manuscript received 22 May 2017; published online 11 August 2017)

In this study, we observe a strong inverse magnetoelectric coupling in $Fe_{52.5}Co_{22.5}B_{25.0}$/PZN-PT multiferroic heterostructure, which produces large electric field (E-field) tunability of microwave magnetic properties. With the increase of the E-field from 0 to 8 kV/cm, the magnetic anisotropy field $H_{\rm eff}$ is dramatically enhanced from 169 to 600 Oe, which further leads to a significant enhancement of ferromagnetic resonance frequency from 4.57 to 8.73 GHz under zero bias magnetic field, and a simultaneous decrease of the damping constant α from 0.021 to 0.0186. These features demonstrate that this multiferroic composite is a promising candidate for fabricating E-field tunable microwave components.

Keywords: ferromagnetic resonance, magnetic anisotropy, magnetoelectric coupling effect, oblique sputtering

PACS: 76.50.+g, 77.55.Nv, 75.30.Gw, 81.15.Cd **DOI:** 10.1088/1674-1056/26/9/097601

1. Introduction

Nowadays, the integration circuit (IC) technology is developing from system-in-a-package toward system-on-a-chip, and the integration of passive components, such as inductors and capacitors, on onechip is critical for miniaturizing the electromagnetic products.[1] Microwave soft magnetic films (SMFs) are key materials for reducing the footprint of magnetic components on monolithic microwave integrated circuit (MMIC) boards.[2,3] The functioning frequency, performances, and size of the magnetic microwave components in MMICs, such as magnetic inductors, phase shifters, circulators, isolators, and filters, primarily dominate ferromagnetic resonance (FMR) frequency $f_{\rm r}$ and the permeability μ of the SMFs.[4–9] The developing trend of MMICs toward high integration, high frequency, light weight, low energy consumption, etc., requires that SMFs should exhibit higher $f_{\rm r}$, larger μ, and good compatibility with IC fabrication processes. On the other hand, in order to reduce the weight and energy consumption of MMICs, researchers are trying to create magnetic devices that can be controlled with no applied magnetic field,[10] that is, the magnetic properties are manipulated with nonmagnetic field methods, such as stress, magnetoelectric coupling, and magnetoelastic coupling, instead of bulky and power-consuming electromagnets.

Metallic soft magnetic films exhibit special advantages in MMICs, because they exhibit higher saturation magnetization $4\pi M_{\rm S}$ and permeability μ, and good compatibility with the IC fabrication processes. Therefore, the self-biased metallic SMFs prepared at IC compatible processes are the recent focus in this area.[11–14] Enhancing uniaxial magnetic anisotropy field $H_{\rm K}$ of SMFs is the most viable route, as it can be increased by 1–2 orders of magnitude, compared to increasing $4\pi M_{\rm S}$ that is capped at 24.5 kG.[11] Various approaches were developed for achieving high $H_{\rm K}$ in SMFs, such as composition gradient sputtering,[12,13,15] oblique sputtering (OS),[16–19] facing target sputtering,[20] exchange coupling,[21–23] and magnetoelectric (ME) coupling.[24–27]

Oblique sputtering is a widely used method for preparing SMFs, because it is easy to tailor the magnetic anisotropy.[16–19] Another effective method to enhance $H_{\rm K}$ is the magnetoelectric coupling in multiferroic composites, which permits electric field manipulation of magnetic properties (inverse ME effect) or magnetic field control of electric polarization (direct ME effect).[24–27] The ME coupling in magnetic/ferroelectric heterostructures can lead to large and E-field tunable $H_{\rm K}$ approaching 750–1100 Oe.[13,28–30] In this study, an SMF with a nominal composition of $Fe_{52.5}Co_{22.5}B_{25.0}$ was deposited on (011)-cut Lead Zinc Niobate–Lead Titanate (PZN-PT) substrate using the OS method at room temperature (an IC compatible process), as shown in Fig. 1. Large and tunable $H_{\rm K}$ up to 600 Oe and $f_{\rm r}$ reaching 8.73 GHz were achieved by E-field manipulation in the $Fe_{52.5}Co_{22.5}B_{25.0}$/PZN-PT multiferroic heterostructure owing to the contribution of both OS and ME coupling.

2. Experimental procedure

As illustrated in Fig. 1, a (011)-cut single crystal PZN-PT substrate with the dimension of 5 mm $[100] \times 5$ mm $[01\bar{1}] \times$

*Project supported by the National Natural Science Foundation of China (Grant No. 11674187).

†Corresponding author. E-mail: lishd@qdu.edu.cn

© 2017 Chinese Physical Society and IOP Publishing Ltd

0.5 mm [011] was pasted onto the sputter chamber's turntable with the [100] and [01$\bar{1}$] directions of PZN-PT along the radial (R) and tangential (T) directions of the turntable, respectively. A $Fe_{52.5}Co_{22.5}B_{25.0}$ film with an average thickness of 100 nm was deposited on the PZN-PT substrate using the OS method at room temperature under 2.8 mTorr Ar atmosphere at a flow rate of 20 sccm, along with an RF power of 80 W and an incidence angle $\theta = 38°$. The magnetic properties were measured using a vibrating sample magnetometer (VSM, PPMS Ever cool II). The microwave performances of the $Fe_{52.5}Co_{22.5}B_{25.0}$/PZN-PT multiferroic heterostructure were evaluated using an FMR spectrometer and a vector network analyzer (Agilent N5224A).

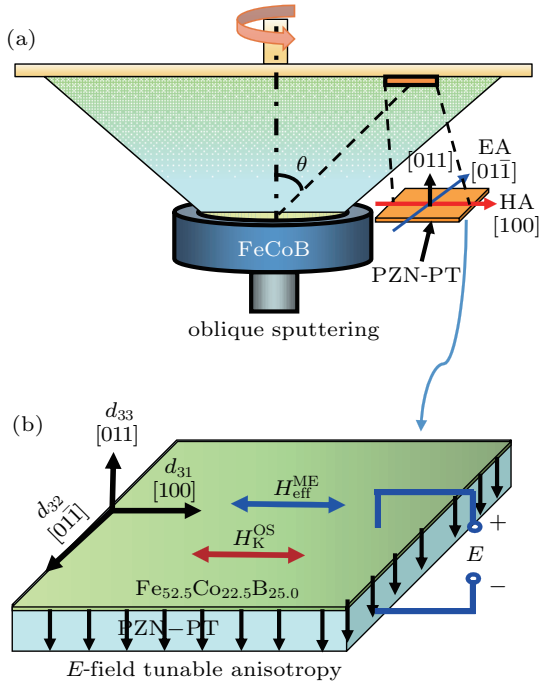


Fig. 1. (color online) Profiles of oblique sputtering device (a) and FeCoB/PZN-PT multiferroic heterostructure (b).

3. Results and discussion

As illustrated in Fig. 2(a), a well-defined uniaxial magnetic anisotropy with a anisotropy field H_K of 169 Oe was observed in the oblique-deposited $Fe_{52.5}Co_{22.5}B_{25.0}$ film with the easy axis (EA) along the tangent direction ([01$\bar{1}$] of the PZN-PT substrate) and hard axis (HA) along the radial direction ([100] of the PZN-PT substrate), respectively. A compressive stress and a tensile stress are generated along the [100] and [01$\bar{1}$] directions of the PZN-PT substrate via the ME coupling effect, respectively.[28–30] For an SMF with a positive magnetostriction coefficient such as λ_S in the studied case, the HA and EA appear along [100] and [01$\bar{1}$] directions, respectively. Thus, the EA directions from the OS and ME coupling are collinear, and the effective anisotropy field H_{eff} is enhanced simultaneously by the OS and ME coupling. Figure 2(b) shows the E-field dependence of the HA hysteresis loops. With the increase of the E-field, the hysteresis loops along the HA||[100] direction of PZN-PT become more difficult to saturate, thereby demonstrating a dramatic enhancement of H_{eff} in $Fe_{52.5}Co_{22.5}B_{25.0}$ induced by the E-field. The E-field-dependent H_{eff} linearly increases from 169 to 600 Oe with the increase of the E-field from 0 to 8 kV/cm, which is equivalent to a large ME tunability of 53.9 Oe·cm/kV.

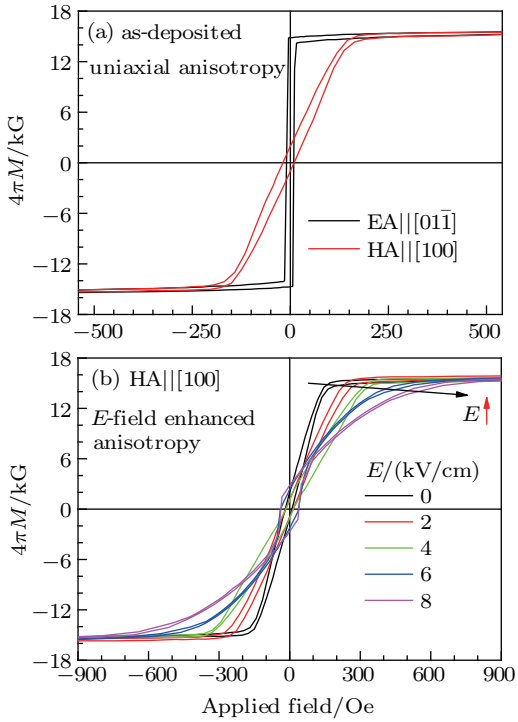


Fig. 2. (color online) Hysteresis loops along EA and HA directions for oblique-deposited $Fe_{52.5}Co_{22.5}B_{25.0}$/PZN-PT multiferroic heterostructure (a), and its E-field dependence of HA hysteresis loops (b).

The exact shift of H_{eff} with the E-field can be established using the FMR spectra. As illustrated in Fig. 3, with the increase of E-field from 0 to 8 kV/cm, the FMR fields H_γ at 11 GHz along the HA||[100] direction are moved upwards from 1026.6 to 1310.4 Oe with an increment of 283.8 Oe, while those along the EA||[01$\bar{1}$] direction are shifted downwards from 887.5 to 601.9 Oe with a decrement of 285.6 Oe. The E-field-induced FMR peak shift can be explained by the strain/stress-mediated in-plane magnetic anisotropy field. The in-plane FMR frequency can be expressed by the Kittel equation

$$f_r = \frac{\gamma}{2\pi}\sqrt{(H_\gamma + H_K + H_{ME})\cdot(H_\gamma + H_K + H_{ME} + 4\pi M_S)}, \quad (1)$$

where H_γ is the measured FMR field, H_K is the anisotropy field induced by OS, and the H_{ME} is the E-field-induced uniaxial magnetic anisotropic field. In the studied case, when an electric field was exerted on a (011)-cut PZN-PT substrate, a compressive stress (σ_c) and a tensile stress (σ_t) were generated along the [100] and [01$\bar{1}$] directions, respectively (see Fig. 1(b)). The total E-field induced stress σ can be expressed

as[28]

$$\sigma = \sigma_t - \sigma_c = \frac{Y}{1+\nu}(d_{32} - d_{31})E, \tag{2}$$

where Y is Young's modulus, ν is Poisson's ratio of the substrate, $d_{31} = -3000$ pC/N along [100], and $d_{32} = 1100$ pC/N along [01$\bar{1}$] are linear anisotropic piezoelectric coefficients of PZN-PT, and E is the applied external electric field. The E-field induced stresses are exerted on ferromagnetic films via interface, thereby leading to a stress-induced magnetic anisotropy field H_{ME}[31]

$$H_{ME} = \frac{3\lambda\sigma}{M_S}, \tag{3}$$

where λ is the magnetostriction coefficient of $Fe_{52.5}Co_{22.5}B_{25.0}$. The stress-mediated magnetoelectric anisotropy field H_{ME} can be obtained by combining Eqs. (2) and (3)[28–30]

$$H_{ME} = \frac{3\lambda Y}{M_S(1+\nu)}(d_{32} - d_{31})E. \tag{4}$$

From Eq. (4), it can be observed that H_{ME} is proportional to the applied E-field, thereby resulting in an electrically enhanced f_r. The Kittel equation (1) on the EA and HA directions can be expressed as follows:

$$f_r^{EA} = \frac{\gamma}{2\pi}\sqrt{\left(H_r^{EA} + H_K^{EA} + H_{ME}^{EA}\right)\cdot\left(H_r^{EA} + H_K^{EA} + H_{ME}^{EA} + 4\pi M_S\right)}, \tag{5}$$

$$f_r^{HA} = \frac{\gamma}{2\pi}\sqrt{\left(H_r^{HA} - H_K^{HA} - H_{ME}^{HA}\right)\cdot\left(H_r^{HA} - H_K^{HA} - H_{ME}^{HA} + 4\pi M_S\right)}. \tag{6}$$

In this study, the effective magnetic field H_{eff} is considerably smaller than $4\pi M_S$. Therefore, equations (5) and (6) can be simplified as

$$f_r^{EA} = \frac{\gamma}{2\pi}\sqrt{\left(H_r^{EA} + H_K^{EA} + H_{ME}^{EA}\right)\cdot 4\pi M_S}, \tag{7}$$

$$f_r^{HA} = \frac{\gamma}{2\pi}\sqrt{\left(H_r^{HA} - H_K^{HA} - H_{ME}^{HA}\right)\cdot 4\pi M_S}. \tag{8}$$

In Eqs. (7) and (8), f_r, H_K, and $4\pi M_S$ are fixed values for the magnetic field scanning FMR measurement, which exhibit no effect with the E-field. Therefore, $H_r^{EA} + H_{ME}^{EA} = C_1$ and $H_r^{HA} - H_{ME}^{HA} = C_2$, where C_1 and C_2 are constants. We can observe that the increase of H_{ME}^{EA} with E-field will lead to a decrease of the measured FMR field H_r^{EA}, that is, H_r along the EA direction is shifted downwards with the increase of the E-field. Similarly, H_r along the HA direction is moved upwards with the increased E-field.

In Eqs. (7) and (8), let $f_r^{EA} = f_r^{HA} = 11$ GHz. Therefore, we can obtain

$$H_r^{EA} + H_K^{EA} + H_{ME}^{EA} = H_r^{HA} - H_K^{HA} - H_{ME}^{HA}. \tag{9}$$

Consequently, the difference of FMR fields along the HA and EA directions are as follows:

$$\begin{aligned}\Delta H_r &= H_r^{HA} - H_r^{EA} \\ &= (H_K^{EA} + H_K^{HA}) + (H_{ME}^{EA} + H_{ME}^{HA}).\end{aligned} \tag{10}$$

The E-field dependence of H_r is summarized in Fig. 3(c). In the case of $E = 0$ kV/cm, the ME coupling field does not exist. Therefore, $\Delta H_r = H_K^{EA} + H_K^{HA}$ suggests that ΔH_r is originated from the uniaxial magnetic anisotropy induced by the B-gradient. In the case of $E = 8$ kV/cm, ΔH_r of 708.5 Oe includes contributions from both the OS stress (193.1 Oe) and the ME coupling effect ($H_{ME}^{EA} + H_{ME}^{HA} = (283.8 + 285.6)$ Oe $=$ 569.4 Oe).

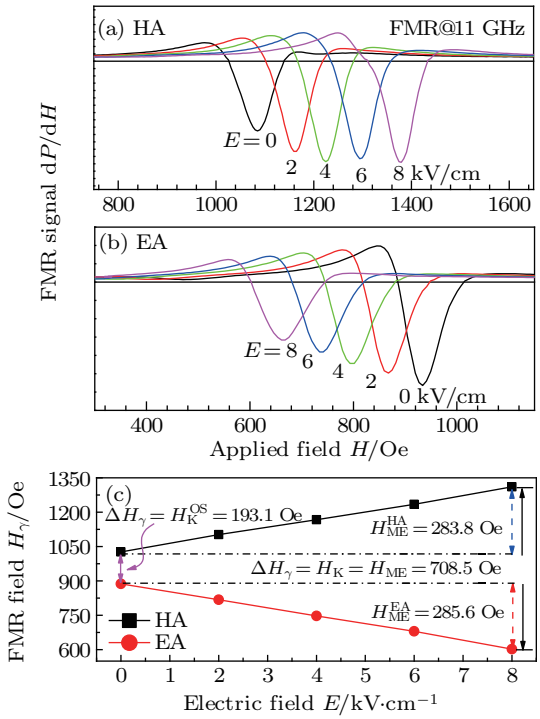


Fig. 3. (color online) E-field dependence of FMR curves at 11 GHz along HA (a) and EA (b) directions, and FMR field H_γ analysis (c).

The large shifts of ΔH_γ under E-fields imply that a large, E-field-controllable f_r is present in the $Fe_{52.5}Co_{22.5}B_{25.0}$/PZN-PT multiferroic heterostructure. Figure 4(a) shows the E-field dependence of the film's permeability. With the increase of the E-field from 0 to 8 kV/cm, the FMR frequencies are shifted from 4.57 to 8.73 GHz with an increment of 4.16 GHz, which is equivalent to an E-field

tunability of 520 MHz·cm/kV. The dependence of $H_{\rm eff}$, $f_{\rm r}$, and α versus E-field are summarized in Fig. 4(b). As discussed earlier, the upward shift of $H_{\rm eff}$ and $f_{\rm r}$ can be attributed to the ME coupling between the $Fe_{52.5}Co_{22.5}B_{25.0}$ film and the PZN-PT substrate. It is interesting to note that the damping constant α decreases from 0.021 to 0.0186 with the increase of E-field, which is considerably favorable for applying $Fe_{52.5}Co_{22.5}B_{25.0}$ films at higher microwave frequencies.

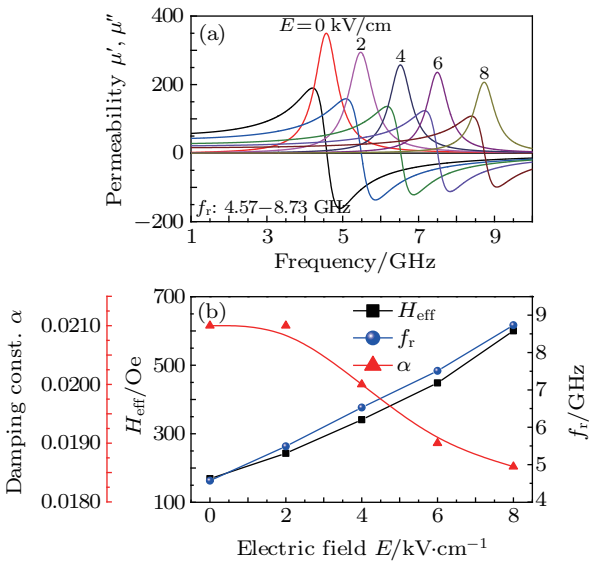


Fig. 4. (color online) Electric field dependence of permeability (a) and $f_{\rm r}$, $H_{\rm eff}$, and α (b).

The ME coupling effect in the $Fe_{52.5}Co_{22.5}B_{25.0}$/PZN-PT multiferroic heterostructure not only generates an FMR shift of 4.16 GHz under an E-field of 8 kV/cm, but also provides an E-field-tunable FMR shift over a considerably wide frequency range, thereby effectively achieving the E-field manipulation on microwave frequencies. It provides a possible route to fabricate E-field tunable microwave devices with large E-field tunability, low energy consumption, and light weight.

4. Conclusion and perspectives

In this study, we obtained the E-field tuning on FMR frequency in as-deposited $Fe_{52.5}Co_{22.5}B_{25.0}$/PZN-PT multiferroic heterostructure owing to the magnetoelectric coupling effect. The heterostructure exhibits large self-biased $f_{\rm r}$ with a considerably wide tunable frequency range from 4.57 to 8.73 GHz, which provides great opportunities for self-biased, voltage-tuned microwave components without high energy-consumption electromagnets. All the fabrication processes are conducted at room temperature (i.e., IC compatible processes), which is considerably beneficial to the integration of soft magnetic films using monolithic microwave integrated circuits.

References

[1] Yamaguchi M, Suezawa K, AraiK I, Takahashi Y, Kikuchi S, ShimadaY, Li W D, Tanabe S and Ito K 1999 *J. Appl. Phys.* **85** 7919
[2] Sun N X and Srinivasan G 2012 *SPIN* **02** 1240004
[3] Luo Y, Eßeling M, Zhang K, Güntherodt G and Samweret K 2006 *Europhys. Lett.* **73** 415
[4] Harris V G 2012 *IEEE Trans. Magn.* **48** 1075
[5] Pardavi-Horvath M 2000 *J. Magn. Magn. Mater.* **215** 171
[6] Yamaguchi M, Suezawa K, Takahashi Y, Arai K I, Kikuchi S, Shimada Y, Tanabe S and Ito K 2000 *J. Magn. Magn. Mater.* **215-216** 807
[7] Li S D, Du J G and Liao C N 2008 *Thin Solid Films* **516** 7748
[8] Shi P, How H, Zuo X, Yoon S D, Oliver S A and Vettoria C 2001 *IEEE Trans. Magn.* **37** 2389
[9] Capraro S, Rouiller T, Berre M L, Chatelon L P, Bayard B, Barbier D and Rousseau J J 2007 *IEEE Trans. Comp. Pack. Tech.* **30** 411
[10] Niemier M 2014 *Nat. Nanotech.* **9** 14
[11] Wang S X, Sun N X, Yamaguchi M and Yabukami S 2000 *Nature* **407** 150
[12] Li S D, Li Q, Xu J, Yan S S, Miao G X, Kang S S, Dai Y Y, Jiao J Q and Lü Y G 2016 *Adv. Funct. Mater.* **26** 3738
[13] Li S D, Xue Q, Duh J G, Du H L, Xu J, Wan Y, Li Q and Lü Y G 2014 *Sci. Rep.* **4** 7393
[14] Jiang C J, Fan X L and Xue D S 2015 *Chin. Phys. B* **24** 057504
[15] Li S D, Huang Z G, Duh J G and Yamaguchi M 2008 *Appl. Phys. Lett.* **92** 092501
[16] Li W D, Kitakami O and Shimada Y 1998 *J. Appl. Phys.* **83** 6661
[17] Yu E, Shim J S, Kim I, Kim J, Han S H, Kim H J and Kim K H 2005 *IEEE Trans. Magn.* **41** 3259
[18] Li C Y, Chai G Z, Yang C C, Wang W F and Xue D S 2015 *Sci. Rep.* **5** 17023
[19] Belyaev B A, Izotov A V and Solovev P N 2016 *Phys. B* **481** 86
[20] Iljinas A, Dudonis J, Bručas R and Meškauskas A 2005 *Nonlinear Analy. Model. Contr.* **10** 57
[21] Lamy Y and Viala B 2005 *J. Appl. Phys.* **97** 10F910
[22] Fetisov Y K and Srinivasan G 2006 *Appl. Phys. Lett.* **88** 143503
[23] Srinivasan G, Zavislyak I V and Tatarenko A S 2006 *Appl. Phys. Lett.* **89** 152508
[24] Spaldin N and Fiebig M 2005 *Science* **309** 391
[25] Eerenstein W, Mathur N D and Scott J F 2006 *Nature* **442** 759
[26] Scott J F 2007 *Nat. Mater.* **6** 256
[27] Vaz C A F, Hoffman J, Anh C H and Ramesh R 2010 *Adv. Mater.* **22** 2900
[28] Lou J, Liu M, Reed D, Ren Y and Sun N X 2009 *Adv. Mater.* **21** 4711
[29] Liu M, Obi O, Lou J, Chen Y J, Cai Z H, Stoute S, Espanol M, Lew M, Situ X D, Ziemer K S, Harris V G and Sun N X 2009 *Adv. Funct. Mater.* **19** 1826
[30] Liu M, Zhou Z, Nan T X, Howe B M, Brown G J and Sun N X 2013 *Adv. Mater.* **25** 1435
[31] Liu X M, Yang R, Du H L, Li Q, Xu J, Wang X, Zong W H, Jin Z J, Zhao G X and Li S D 2017 *Thin Solid Films* **636** 15